Phase I, first-in-human study of XTR004, a novel 18F-labeled tracer for myocardial perfusion PET: biodistribution, radiation dosimetry, pharmacokinetics and safety after a single injection at rest

Chao Ren
Peking Union Medical College Hospital
Qingqing Pan
Peking Union Medical College Hospital
Chao Fu
Peking Union Medical College Hospital
Peipei Wang
Peking Union Medical College Hospital
Zhiquan Zheng
zqzheng@bucm.edu.cn

Sinotau Pharmaceutical Group
Bailing Hsu
University of Missouri Columbia Health Care: MU Health Care
Li Huo
Peking Union Medical College Hospital https://orcid.org/0000-0003-1216-083X

Research Article

Keywords: positron emission tomography, 18F-labeled MPI tracer, XTR004, pharmacokinetics, radiation dosimetry, myocardial ischemia, coronary heart disease.

Posted Date: January 3rd, 2023

DOI: https://doi.org/10.21203/rs.3.rs-2406961/v1

Version of Record: A version of this preprint was published at Journal of Nuclear Cardiology on February 1st, 2024. See the published version at https://doi.org/10.1016/j.nuclcard.2024.101823.

Abstract

Purpose: XTR004 is a novel ^{18}F-labeled myocardial perfusion imaging tracer that can be clinically used to assess myocardial ischemia from coronary artery disease. This study aimed to evaluate imaging characteristics of XTR004 after a single injection at rest in humans.

Methods: Eleven healthy subjects (man=8) received an intravenous injection of 239-290 MBq (6.5-7.8 mCi) XTR004 and imaged with nine whole-body positron emission tomography (PET) scans within 4.7 h. Collection of blood and urine samples was concurrently performed for 7.25 h. Image processing utilized 3D registered PET and CT images to derive %ID and then calculated the radiation dose using a Hermes workstation with the embedded OLINDA/EXM program. The radioactive count profile was measured for whole-blood, plasma, and urine to characterize pharmacokinetics with the metabolic correction. The safety profile was evaluated during the day of dosing and three follow-up visits, including physical examination, vital signs, laboratory tests and adverse event observation.

Results: Myocardial uptake of XTR004 was rapid, high, and stable throughout the PET imaging period. In the 0-12 min PET images, the top five organs of %ID were liver (26.81±4.01), kidney (11.43±2.49), lung (6.75±1.76), myocardium (4.72±0.67) and spleen (3.1±0.84). Mean values of C_{max}, T_{max}, $t_{1/2}$, and $AUC_{0\text{-}last}$ calculated by the non-compartment model in corrected plasma were 0.0013896 %ID/g, 2.543 min, 45.171 min, and 0.03314 min* (%ID/g), respectively. Whole-body effective dose per unit of injected activity was 0.0165 mSv/MBq. Cumulative urine excretion (Cum Ae) was 8.18%. Treatment-related adverse events occurred in seven subjects (63.6%) and were overall reported as stimulated pain at the injection site. No severe adverse event was collected.

Conclusions: XTR004 having a favorable safety profile with rapid, high, and stable myocardial uptake in humans demonstrated an excellent potential for PET MPI. Further exploration of XTR004 PET MPI to detect myocardial ischemia can be warranted. (A Study of XTR004 PET Radiotracer in Healthy Volunteers, ClinicalTrials.gov number NCT05195879.)

Introduction

Ischemic heart disease (IHD) is a type of chronic diseases to cause a high mortality rate around the world [1]. In 2020, 244.1 million people worldwide experienced IHD with a mortality rate of 112.37/100,000 [2]. In 2021, 330 million people in China carry relevant risk factors to develop IHD, and 11.39 million patients were diagnostically confirmed IHD [3]. During 2019, the mortality rate of IHD in China has reached 121.59/100,000 in urban areas and 130.14/100,000 in rural areas to create a heavy burden to the Chinese communities [4]. Myocardial perfusion imaging (MPI) has been worldwide established as an important clinical tool to perform noninvasive diagnosis and risk stratification for myocardial ischemia due to IHD, and to guide patient management [5–9]. In recent decades, it has been proved that positron computed tomography (PET) MPI outperforms single photon emission computed tomography (SPECT) MPI for the detection of myocardial ischemia in conjunction of the advantage of absolute myocardial blood flow quantification [10–12]. The clinical application of PET MPI has gradually increased [13–14]. Currently, PET MPI tracers including ^{82}Rb, ^{15}O-H_2O, and ^{13}N-Ammonia are overall with relatively short physical half-life (75 sec to 10 min). Consequently, either an on-site generator or a cyclotron is demanded for tracer production. This requisite results in high initial or on-going cost for tracer production, thus limiting the capability to further widespread the clinical utilization [15–16]. The use of PET MPI tracers with a longer half-life isotope (e.g. ^{18}F, 109.8 min) has therefore become an important solution to overcome the disadvantage of current MPI tracers [17]. Among ^{18}F-labeled tracers, flurpiridaz F18 (formerly known as BMS747158-02) is the most well-known one which has just completed its Phase III clinical trial in May 2022 and will soon be launched in Europe and USA market in 2023. Flurpiridaz encompassing excellent imaging characteristics for MPI include: 1) rapid myocardial uptake through fast binding to mitochondrial respiratory complex I (MC-I) chain [18]; 2) the closely linear relationship between myocardial uptake and myocardial blood flow, thus enhancing the sensitivity in the detection of mild to moderate myocardial ischemia as compared to SPECT MPI [19, 20–21]. XTR004 (known as ^{18}F-FMMP2) containing a main chemical structure to that of flurpiridaz has been first introduced as another ^{18}F-labeled PET MPI tracer in 2016 [22]. The major difference is characterized by the molecule of PEGylated benzyl triazole as a side chain linked to the main structure (Fig. 1). Like flurpiridaz, XTR004 belonging to the category of MC-I inhibitors can also achieve rapid binding to the MC-I raspatory complex with a long retention in the myocardium [23]. As a labeled Class-I drug, XTR004 is currently undergoing regulated clinical trials in China. This study reported the first human clinical trial of XTR004 to evaluate its biological distribution, radiation dosimetry, pharmacokinetics, and the safety after a single intravenous (IV) bolus injection at rest.

Materials And Methods

Research Design

The study was a single-center, single-arm, non-randomized, open Phase I clinical trial (NCT05195879) conducted at the Peking Union Medical College Hospital with an ethical approval followed by the Declaration of Helsinki. Eleven healthy participants were recruited from March 2021 to July 2021, and underwent the screening process of enrolment. All subjects underwent a physical examination, vital sign assessment and

relevant laboratory tests, and further examinations with clinical electrocardiograph (ECG), echocardiography and electroencephalogram (EEG). On the day of dosing XTR004, subjects received an IV bolus injection of XTR004. Subsequently, whole-body PET images were acquired, and blood and urine samples were collected simultaneously within multiple periods. Multiple sessions of physical examination, vital sign assessment, and ECG monitoring were performed accordingly. After the day of dosing, two prescheduled on-site visits (next day and 7 days after) were conducted for the safety monitoring, including physical examination, vital sign assessment, and related laboratory tests, and adverse event collection. A follow-up phone call was performed on the 14th day to complete the investigatory process.

Inclusion/exclusion Criteria

The enrolment of healthy adults required ages from 18 to 40 years old who should be qualified by medical history, physical examination, vital signs, echocardiography, ECG, EEG, and laboratory tests. The inclusion criteria were: male or female, no current use of drugs, and normal laboratory tests or abnormal results without clinical significance. All subjects agreed to take effective contraception during the study period and after for 6 months. The exclusion criteria were: any serious heart or brain disease, other major diseases, prescheduled surgery and other invasive interventions one week after dosing; a history of liver or gastrointestinal disease or other conditions that may interfere drug absorption, distribution, excretion, or metabolism as determined by the investigator; a history of high-risk or severe allergic reactions to medications; significant occupational exposure to ionizing radiation within the past 10 years or for therapeutic purposes or research purposes other than this study; other conditions that investigators consider inappropriate to participate in the trial.

Pet Tracer Administration

On the day of dosing, each subject received an IV bolus injection (5 sec) of XTR004 with a targeted dose of 222–296 MBq (6.0–8.0 mCi) in a volume of 1–3 mL. After the IV injection, a 3–5 mL saline flush immediately followed. The net dose was calculated by subtracting the prepared dose calibrated with the residual activity in the syringe and tube line after injection as both activities were calibrated to the injection time.

Pet/ct Imaging

In this study, a Polestar m680 PET/CT scanner (Sinogram Union, Beijing, China) was utilized to acquired multiple whole-body CT and PET scans covering form top of the head to the upper 1/3 thigh. After appropriate positioning, subjects underwent the first low-dose CT scan (55 mA, 120 keV) for PET attenuation correction and image fusion. Within 5 h after the tracer injection, three CT scans (before 0–12 min, 120–132 min and 240–252 min) and nine 3D PET scans (0–12 min, 12–24 min, 24–36 min, 36–48 min, 48–60 min, 120–132 min, 150–162 min, 240–252 min, and 270–282 min) were acquired. PET image reconstruction utilized an iterative reconstruction algorithm integrated with necessary physical corrections to convert each pixel value to radiation concentration with an unit of (Bq/mL).

Measurement Of Bio-distribution And Radiation

An open-source software (Amide) for PET-CT imaging analysis was used to measure the standardized uptake value (SUV) of each organ (brain, salivary gland, thyroid, myocardium, liver, lung, gallbladder wall, pancreas, kidney, muscle, small intestine, upper large intestine, red bone marrow, spleen, testis, bladder, and uterus) at different time points [24]. The processing steps included the use of CT images to register corresponded PET images manually for identifying organs on PET images. SUV values were measured with multiple preset regions of interest (ROI), depending on the geometrical size of an organ. The %ID for key organs with high uptake and the whole body were measured using the Hermes image processing workstation using a single CT scan to register all PET scans. 3D contours for key organs were drawn manually and then applied to generate time-dependent %IDs. The residence time was generated using a mono exponential model and the non-linear curve fitting. For the internal dosimetry, the OLINDA/EXM software was utilized to calculate the absorbed and effective doses for each organ and whole-body. To understand the radiation exposure of XTR004 injection to the clinical environment, the accumulated radiation dose during the day of dosing, including PET imaging technologists, medical nurses, and blood drawing nurses were monitored with radiation dosimeters.

Measurement Of Radioactivity In Blood And Urine

An IV setting of blood collection was preinstalled in the dorsal hand vein or cubital vein of the subject. A total of 54 ml of venous blood were collected at 9 time points (1.5, 3, 5, 10, 30, 60, 120, 240, and 420 min after administration) as 6 mL for each time point. A volume of 1 ml was drawn for each blood samples (whole-blood) and placed in a counting tube to weigh with a ultrafine scale and to measure radioactive counts (cpm) with a well counter. The remaining 5 mL sample was centrifuged, and a 0.5 mL supernatant was moved into the counting tube to weigh and to measure radioactive counts (cpm). The percentage of injected dose per gram (%ID/g) was calculated by normalizing radioactive counts of whole-blood or plasma to counts of a 1/10000 diluted tracer in 0.5 ml volume. Time activity curves (TAC) of whole-blood and plasma were

plotted to calculate the whole-blood/plasma radioactivity ratio. The remaining plasma was analyzed with a radio-RP-HPLC to derive the proportion of ^{18}F-labeled prototype and metabolites for metabolic correction in the sequent pharmacokinetic analysis. Urine samples were collected in four periods (0–75 min, 76–135 min, 136–300 min, and 301–435 min after drug administration), and weighed and processed to measure urine radioactive counts. The proportion of ^{18}F-labeled prototype in the urine was analyzed to examine urine excretion.

Safety Assessment

Safety monitoring was carried out on the day of dosing, and 2, 7, and 14 days after dosing. The measurement of safety profile include: measurements of heart and brain with multiple 12-lead ECGs and EEGs; measurement of troponin I levels before and after dosing. The safety assessment also contained to record adverse and serious adverse events after a single intravenous bolus injection of XTR004. Abnormal changes relative to baseline in vital signs, physical examination, clinical laboratory tests (routine blood, biochemistry, and urinalysis), ECG, and EEG were determined by the investigator to verify if clinical significance.

Statistical Analysis

Descriptive statistics for SUV, %ID, radiation dose, effective dose, and myocardial residence time of each organ were presented for each time point of PET imaging. Descriptive statistics for whole blood and plasma radioactivity concentrations and the ratio of whole blood/plasma radioactivity concentration were also calculated. C_{max}, T_{max}, $t_{1/2}$, AUC, Cum fe, CLr, and other parameters were further derived using a non-compartmental model with the Phoenix WinNonlin software (Certara, L.P., version 8.3). Descriptive statistics were performed for the pharmacokinetic parameters of whole blood, plasma, metabolically corrected plasma, and urine. Descriptive analyses of baseline and post-administration results were performed, and adverse event rates were summarized according to the number and percentage of subjects with adverse events. All statistical analyses were completed with the SAS software (SAS Institute, Inc., version 9.4).

Results

Demographic Characteristics

Eleven subjects enrolled in the study (nine males and two females) received XTR004 and completed all safety assessments. One subject showed an injection issue; therefore, the PET data of this subject were excluded from the subsequent data analysis. The mean age of ten remaining subjects was 29.1 ± 4.6 years, and the mean body mass index was 22.3 ± 2.75 kg/m^2.

Biological Distribution

The mean injected dose of XTR004 was 270.27 MBq (7.30 mCi) and ranged from 239 to 290 MBq (6.5–7.8 mCi) with an average chemical dose of 1.06 ± 0.53 μg in a single administration. Whole-body multisite PET imaging over nine time periods clearly showed the distribution of radioactivity in organs as presenting the biodistribution of XTR004 in human body. The %ID of each organ is listed in Table 1. Liver had the highest uptake (26.81 ± 4.01%ID) in the first whole-body PET imaging (0–12 min after administration), followed by the kidney (11.43 ± 2.49%ID), lung (6.75 ± 1.76%ID), myocardium (4.72 ± 0.67%ID), and spleen (3.10 ± 0.84%ID). The %ID of the liver reached the maximum value of 31.78%ID during 12–24 min, decreased to 11.86%ID during 120–132 min (△=19.92%ID, decreasing rate DR = 62.68%), and further decreased to 8.04%ID during 270–282 min (△=3.82%ID, 32.21%). Within 12–282 min, the total descending gradient in liver was 23.74% (74.70%). The %ID of kidney reached the maximum value of 11.43%ID at 0–12 min, decreased to 3.79%ID at 48–60 min (△=7.64%ID, 66.84%), and further decreased to 2.08%ID at 270–282 min (△=1.71%ID, 45.12%). Within 0–282 min, the overall descending gradient in kidney was 9.43 g/mL (82.50%). The %ID of lung reached the maximum value of 6.75% at 0–12 min and decreased to 2.15% at 270–282 min (△=4.6%ID, 68.15%). Myocardial uptake remained stable within 60 min after IV injection (variation = 7.2%). Myocardium reached the maximum value of 4.72%ID in 0–12 min, slightly decreased to 4.38%ID in 48–60 min, and then followed a significant decrease after. During 0–282 min, the total descending gradient was 1.87%ID (39.62%) to give an residence time as 0.0691 ± 0.0112 h. The %ID of the spleen reached a maximum value of 3.10% at 0–12 min and decreased to 0.69% at 270–282 min (△=2.41%ID, 77.74%). SUV for each organ is shown in Table 2. The top five organs of SUV in the first whole-body PET imaging (0–12 min of administration) were kidney (15.18 ± 3.48 g/mL), liver (9.65 ± 1.73 g/mL), spleen (8.25 ± 1.38 g/mL), myocardium (7.06 ± 1.29 g/mL), and pancreas (7.04 ± 2.84 g/mL). Myocardium and other organs showed SUV changes similar to %ID changes. Figure 2 shows a subject with rapid, high, and stable myocardial uptake of XTR004 throughout PET scans. Liver uptake was initially high with significant washout approximately 60 min later. The radioactivity in the blood pool of whole body gradually increased corresponding with the washout in liver. The radioactivity in small intestine gradually increased during 120–132 min and 150–162 min, and gradually decreased during 240–252 min and 270–282 min. The radiation activity of large intestine (ascending and transverse colon) continued to increase after 150–162 min, suggesting that XTR004 could be excreted through the intestine. The kidney showed high radioactive activity,

followed by rapid clearance, and the accumulation of radioactive urine in the bladder increased with time, indicating that XTR004 can also be excreted through urine pathway.

Table 1

Percentage decay-corrected administered ^{18}F dose (%ID) versus time after dosing (mean ± SD, n = 10)

Organ	Time (min)								
	0–12	12–24	24–36	36–48	48–60	120–132	150–162	240–252	270–282
Brain	1.22 ± 0.57	1.34 ± 0.51	1.58 ± 0.58	1.75 ± 0.63	1.89 ± 0.62	2.47 ± 0.75	2.5 ± 0.75	2.82 ± 0.75	2.79 ± 0.84
Gallbladder wall	0.15 ± 0.08	0.2 ± 0.12	0.19 ± 0.12	0.17 ± 0.11	0.17 ± 0.13	0.12 ± 0.1	0.11 ± 0.08	0.12 ± 0.1	0.11 ± 0.12
Heart wall	4.72 ± 0.67	4.28 ± 0.58	4.45 ± 0.71	4.42 ± 0.71	4.38 ± 0.64	3.87 ± 0.45	3.59 ± 0.45	2.98 ± 0.43	2.85 ± 0.43
Kidneys	11.43 ± 2.49	7.47 ± 1.39	5.37 ± 0.92	4.32 ± 0.71	3.79 ± 0.59	2.46 ± 0.58	2.25 ± 0.47	2.06 ± 0.58	2.08 ± 0.53
Liver	26.81 ± 4.01	31.78 ± 2.76	29.87 ± 2.45	26.65 ± 2.6	22.92 ± 2.9	11.86 ± 1.84	10.09 ± 1.29	8.6 ± 1.12	8.04 ± 1.01
Lungs	6.75 ± 1.76	3.37 ± 0.85	2.72 ± 0.7	2.44 ± 0.58	2.36 ± 0.53	2.2 ± 0.62	2.18 ± 0.57	2.16 ± 0.62	2.15 ± 0.62
Pancreas	1.94 ± 0.82	1.54 ± 0.66	1.24 ± 0.6	1.01 ± 0.49	0.9 ± 0.46	0.51 ± 0.31	0.49 ± 0.29	0.42 ± 0.27	0.47 ± 0.31
Red marrow	3.03 ± 1.22	3.36 ± 1.02	3.43 ± 1.02	3.42 ± 1.05	3.44 ± 1.08	3.26 ± 1.06	3.4 ± 1.08	3.18 ± 1.15	3.35 ± 1.18
Salivary	0.19 ± 0.07	0.2 ± 0.07	0.21 ± 0.07	0.21 ± 0.06	0.21 ± 0.07	0.2 ± 0.08	0.19 ± 0.06	0.18 ± 0.08	0.16 ± 0.07
Small intestine	0.19 ± 0.08	0.18 ± 0.08	0.18 ± 0.07	0.17 ± 0.07	0.17 ± 0.07	0.18 ± 0.11	0.16 ± 0.08	0.15 ± 0.06	0.16 ± 0.09
Spleen	3.1 ± 0.84	1.12 ± 0.34	0.81 ± 0.22	0.72 ± 0.21	0.71 ± 0.21	0.64 ± 0.18	0.63 ± 0.2	0.65 ± 0.27	0.69 ± 0.25
Testes	0.07 ± 0.06	0.23 ± 0.18	0.29 ± 0.21	0.35 ± 0.22	0.39 ± 0.25	0.48 ± 0.22	0.51 ± 0.25	0.49 ± 0.23	0.54 ± 0.31
Thyroid	0.36 ± 0.13	0.32 ± 0.1	0.32 ± 0.12	0.34 ± 0.12	0.34 ± 0.12	0.36 ± 0.12	0.34 ± 0.11	0.33 ± 0.12	0.31 ± 0.11
Upper large intestine wall	0.74 ± 0.42	0.7 ± 0.34	0.66 ± 0.32	0.6 ± 0.3	0.56 ± 0.27	0.36 ± 0.17	0.33 ± 0.17	0.31 ± 0.18	0.3 ± 0.14
Urinary bladder	0.38 ± 0.27	1.06 ± 0.23	1.74 ± 0.27	2.49 ± 0.43	3.35 ± 0.49	1.96 ± 1.11	3.27 ± 1.1	2.12 ± 3.22	2.99 ± 3.55
Uterus	0.22 ± 0.19	0.36 ± 0.11	0.61 ± 0.36	0.72 ± 0.41	0.89 ± 0.6	0.53 ± 0.01	1.11 ± 0.23	0.45 ± 0.05	0.76 ± 0.07

Table 2
SUV (g/mL) versus time after dosing (mean ± SD, n = 10)

Organ	Time (min)								
	0–12	12–24	24–36	36–48	48–60	120–132	150–162	240–252	270–282
Brain	0.34 ± 0.1	0.4 ± 0.09	0.46 ± 0.09	0.49 ± 0.11	0.55 ± 0.1	0.64 ± 0.1	0.65 ± 0.08	0.69 ± 0.1	0.71 ± 0.1
Gallbladder wall	3.84 ± 1.91	4.09 ± 0.89	4.19 ± 1.4	6.2 ± 5.72	6.58 ± 6.06	8.07 ± 7.39	7.96 ± 8.17	7.75 ± 7.2	8.19 ± 8.22
Heart wall	7.06 ± 1.29	6.89 ± 1.67	6.89 ± 1.81	7.1 ± 1.89	6.64 ± 1.71	5.11 ± 1.58	4.5 ± 1.19	3.04 ± 0.88	2.69 ± 1.01
Kidneys	15.18 ± 3.48	9.02 ± 2.76	5.85 ± 1.78	4.21 ± 0.79	3.43 ± 0.7	1.94 ± 0.37	1.75 ± 0.41	1.33 ± 0.36	1.34 ± 0.29
Liver	9.65 ± 1.73	12.31 ± 2.56	11.21 ± 3.3	9.54 ± 3.08	8.1 ± 3.08	3.64 ± 1.3	3.03 ± 1.04	2.18 ± 0.58	2.11 ± 0.63
Lungs	1.55 ± 0.56	0.71 ± 0.36	0.44 ± 0.14	0.38 ± 0.12	0.41 ± 0.16	0.36 ± 0.24	0.37 ± 0.25	0.25 ± 0.09	0.25 ± 0.1
Muscle	0.36 ± 0.19	0.76 ± 0.51	0.88 ± 0.51	0.92 ± 0.47	1.07 ± 0.47	1.32 ± 0.43	1.4 ± 0.48	1.35 ± 0.46	1.37 ± 0.48
Pancreas	7.04 ± 2.84	5.39 ± 1.9	4.01 ± 1.26	2.96 ± 0.9	2.6 ± 0.8	1.07 ± 0.23	1.16 ± 0.26	0.81 ± 0.25	0.89 ± 0.17
Red marrow	1.51 ± 0.76	2.04 ± 0.78	1.99 ± 0.51	1.78 ± 0.51	1.76 ± 0.45	0.92 ± 0.19	0.83 ± 0.13	0.68 ± 0.17	0.7 ± 0.24
Salivary	2.32 ± 0.77	2.61 ± 0.85	2.5 ± 0.67	2.47 ± 0.63	2.46 ± 0.79	2.32 ± 1.03	2.14 ± 0.99	2.06 ± 0.85	1.91 ± 0.85
Small intestine	2.26 ± 0.64	2.05 ± 0.59	1.84 ± 0.53	1.67 ± 0.51	1.56 ± 0.48	1.36 ± 0.39	1.21 ± 0.38	1 ± 0.33	0.89 ± 0.28
Spleen	8.25 ± 1.38	2.63 ± 0.57	1.59 ± 0.26	1.34 ± 0.17	1.21 ± 0.16	0.87 ± 0.29	0.84 ± 0.21	0.79 ± 0.25	0.84 ± 0.17
Testes	0.13 ± 0.09	0.64 ± 0.21	0.8 ± 0.2	0.91 ± 0.26	1.02 ± 0.32	1.1 ± 0.23	1.18 ± 0.31	1.18 ± 0.38	1.11 ± 0.21
Thyroid	3.82 ± 1.1	1.98 ± 0.65	2.1 ± 0.65	2.13 ± 0.71	2.11 ± 0.71	1.94 ± 0.43	1.86 ± 0.53	1.86 ± 0.39	1.77 ± 0.38
Upper large intestine wall	5.52 ± 0.83	5.18 ± 0.77	4.61 ± 0.95	4.21 ± 1.02	3.74 ± 0.93	2.2 ± 0.72	1.81 ± 0.52	1.49 ± 0.45	1.33 ± 0.42
Urinary bladder	2 ± 1.38	14.15 ± 21.23	19.49 ± 23.41	19.78 ± 22.84	20 ± 20.01	17.03 ± 9.2	16.92 ± 11.32	10.12 ± 6.16	9.01 ± 6.05
Uterus	1.43 ± 0.46	1.65 ± 0.44	1.65 ± 0.15	1.16 ± 0.13	1.28 ± 0.31	1.11 ± 0.17	1.39 ± 0.01	1.86 ± 1.04	2.98 ± 2.37

Radiation Dosimetry

Absorbed radiation doses (μSv/MBq) are summarized in Table 3. The thyroid (54.9 μSv/MBq) had the highest absorbed dose, followed by the kidney (49.53 μSv/MBq), liver (49.23 μSv/MBq), myocardium (45.16 μSv/MBq), and bladder wall (44.59 μSv/MBq). The corresponding effective doses for each organ are shown in Fig. 3. After IV injection of XTR004, the top five organs with effective radiation doses were thyroid (2.20 μSv/MBq), liver (1.97 μSv/MBq), bladder wall (1.78 μSv/MBq), testis (1.57 μSv/MBq), and lung (1.54 μSv/MBq). The whole-body effective dose per unit of injection activity was 0.0165 mSv/MBq. When the actual IV dose was 7.30 mCi, a subject received an effective dose of 4.474 mSv. Radiation doses received by PET imaging operators, medical nurses, and blood drawing nurses were 0.86 ± 0.21 μSv, 5.63 ± 11.90 μSv, and 10.86 ± 4.03 μSv, respectively.

Table 3
Absorbed dose estimates (μSv/MBq) for the void interval of 4.5 h (n = 10)

Organ	Mean (n = 10)	SD	Minimum	Maximum
Adrenals	1.94E + 01	3.97E-03	1.49E + 01	2.71E + 01
Brain	9.78E + 00	3.18E-03	6.40E + 00	1.80E + 01
Breasts	1.78E + 00	3.79E-03	0.00E + 00	1.00E + 01
Gallbladder wall	2.33E + 01	6.89E-03	1.74E + 01	3.98E + 01
Heart wall	4.52E + 01	9.37E-03	3.29E + 01	6.48E + 01
Kidneys	4.95E + 01	1.98E-02	2.90E + 01	8.29E + 01
Liver	4.92E + 01	9.14E-03	3.91E + 01	6.45E + 01
Lower large intestine wall	1.01E + 01	2.49E-03	7.80E + 00	1.61E + 01
Lungs	1.29E + 01	2.65E-03	9.40E + 00	1.73E + 01
Osteogenic cells	9.68E + 00	1.95E-03	7.90E + 00	1.42E + 01
Ovaries	2.70E + 00	5.79E-03	0.00E + 00	1.57E + 01
Pancreas	2.77E + 01	1.01E-02	1.34E + 01	4.73E + 01
Red marrow	1.23E + 01	3.28E-03	8.90E + 00	1.96E + 01
Salivary	1.12E + 01	3.45E-03	8.40E + 00	1.92E + 01
Small intestine	1.02E + 01	2.35E-03	8.20E + 00	1.57E + 01
Spleen	2.97E + 01	2.23E-02	1.24E + 01	9.07E + 01
Stomach wall	1.15E + 01	1.98E-03	9.30E + 00	1.60E + 01
Testes	3.88E + 01	3.26E-02	0.00E + 00	1.14E + 02
Thymus	1.00E + 01	1.99E-03	7.80E + 00	1.47E + 01
Thyroid	5.49E + 01	1.88E-02	2.80E + 01	9.50E + 01
Total body	8.65E + 00	2.28E-03	6.70E + 00	1.40E + 01
Upper large intestine wall	1.51E + 01	2.22E-03	1.27E + 01	1.91E + 01
Urinary bladder	4.46E + 01	4.51E-02	2.05E + 01	1.71E + 02
Uterus	9.71E + 00	2.19E-02	0.00E + 00	6.53E + 01
Effective dose	1.65E + 01	3.91E-03	1.25E + 01	2.30E + 01

Safety

No SAE occurred during the study. Treatment emergent adverse event (TRAE) was reported in seven subjects (63.6%), and all of them reported pain at the injection site due to the presence of slight alcohol in the study drug (10% of injection volume, 0.1–0.5 mL). No medical action were taken for any AE, and subjects recovered without any treatment. After IV injection of XTR004, laboratory parameters such as routine blood, blood biochemistry, urine routine, coagulation function, serum virus blood screening, blood troponin I, pregnancy test, and EEG and ECG results showed no clinically significant changes over time, and no trend or signal of safety issues was found. In terms of vital signs and physical examination, all of them were within the normal range. Regarding ECG findings, one subject had a nonspecific 12-lead ECG abnormality during the screening period, identified as a left posterior fascicular block and a first-degree atrioventricular block. This subject still had a first-degree atrioventricular block on the day of administration and at the visit on day 7 after administration. The investigator observed that the abnormal ECG was related to the subject's condition as unrelated to the study drug; therefore, no medical action was taken for this AE.

Pharmacokinetics

The radioactive TAC of whole blood, plasma, and metabolically corrected plasma are shown in Fig. 4. The ratio of whole blood and plasma radioactivity concentrations ranged from 0.5967 to 0.7952. After IV injection of XTR004, plasma radioactivity rapidly peaked at

0.0013273%ID/g at 3 min, decreased to 0.0006395%ID/g at 30 min (a decrease rate of 51.82%), and then continued to boost. Results of the radio-RP-HPLC analysis showed that the mean ratio of the XTR004 prototype drug was 99.60%, 99.54%, 92.52%, and 77.85% at 1.5 min, 3 min, 30 min, and 60 min. After 120 min, the plasma radioactive concentration for subjects was lower than the detectable limit of radio-RP-HPLC. Mean values of C_{max}, T_{max}, $t_{1/2}$, and AUC_{0-last} calculated by the non-compartment model were 0.0013896%ID/g, 2.543 min, 45.171 min, and 0.03314 min* (%ID/g), respectively. Mean value of $AUC_{0-\infty}$ was 0.02760 min × (%ID/g). The mean cumulative urine excretion Cum Ae, cumulative excretion rate Cum fe, and renal clearance CLr were 8.18%ID, 8.18%, and 21.3 g/min. Prototype of XTR004 was not detectable in urine samples.

Discussion

Biological distribution

As a ^{18}F-labeled PET MPI tracer, XTR004 has biological distribution (%ID) similar to those of flurpiridaz [25]. Top five organs with high ID% in the first PET scan (0–12 min) after XTR004 administration were liver (26.81%ID), kidney (11.43%ID), lung (6.75%ID), myocardium (4.72%ID), and spleen (3.10%ID). Similarly, top five organs in the first PET scan (10–30 min) after flurpiridaz administration were liver (19.1%ID), kidney (9.4%ID), brain (8.3%ID), myocardium (3.1%ID), and stomach wall (2.5%ID). The main difference was low uptake of XTR004 in the brain (1.22%ID) in comparison to that of flurpiridaz (8.3%ID). The reason is that XTR004 with the PEGylated benzyl triazole structure in the side chain created a high hydrophilicity that made XTR004 difficult to cross the blood-brain barrier [26]. During the entire PET scan period (0–282 min), the myocardial uptake of XTR004 was rapid, high, and stable similar to that of flurpiridaz (Fig. 5) to give close residence time of 0.0691 and 0.0782 (h). These values were higher than those of current PET MPI tracers having short half-life (^{13}N-Ammonia, ^{82}Rb, and ^{15}O-H_2O), but lower than that of the current SPECT tracer, ^{99m}Tc-Sestamibi (Table 4) [27–30]. Liver uptake of XTR004 and flurpiridaz peaked at 10–30 min after IV administration and continuously decreased until 60 min. As both tracers metabolized by the liver acoordingly, the radioactivity in the blood stream continued increasing after 60 min. Renal uptake of XTR004 and flurpiridaz peaked in the first PET scan and decreased gradually to accumulate in the bladder, suggesting urinary excretion for both tracers (Fig. 2 and reference 25).

Table 4
The myocardial residence time of MPI tracers injected at rest.

Radiopharmaceuticals used for MPI	^{13}N-ammonia [28]	^{82}Rb [29]	^{15}O-H_2O [30]	^{99m}Tc-sestamibi [27]	Flurpiridaz [25]	XTR004
Injection dose (MBq)	555 ~ 740	999.1 ± 200.1	880 ~ 2280	296 ~ 370	170 ~ 244	270.27 ± 18.88
Residence times (h)	0.00388	0.00051	0.000927	5.18	0.0728	0.0691

Although the uptake of XTR004 in the myocardium and liver was higher than that of flurpiridaz, the myocardium/liver ratio of both was quite similar (ranging from 0.16 to 0.36 within 120 min), and lower than that of the SPECT imaging tracer ^{99m}Tc-Sestamibi (0.4–1.7 within 120 min) (Fig. 5). Nonetheless, due to the high spatial resolution of PET imaging, instantaneous imaging post tracer injection could still provide high-quality PET images for the diagnostic purpose [20–21]. Dynamic PET data for the quantitative analysis of myocardial blood flow that can further enhance the CAD diagnosis [31–32]. Although ^{99m}Tc-Sestamibi has a higher myocardium/liver ratio, the spillover from liver into myocardium can be more prominent due to the low spatial resolution of SPECT [33]. It is recommended that high-quality SPECT images can only be obtained after the significant washout of liver uptake (approximately 1 h after injection) [9]. Currently, only a few models of SPECT devices can perform dynamic SPECT imaging, thus the application of myocardial blood flow quantiation with ^{99m}Tc-labeled SPECT tracers is still in the stage of clinical research.

Pharmacokinetics

The change in the plasma radiation concentration of XTR004 after IV injection was mainly related to liver metabolism. By comparing the biological distribution of liver with the radioactive concentration in the blood, both the decrease in liver uptake toward the valley and the initialized increase of plasma radioactivity occurred approximately at 30 min after administration. With the liver metabolism continued, the radiation concentration in blood increased to reach 0.0010599%ID/g at 240 min (79.85% of the original peak). Although no relevant blood pharmacokinetic data for flurpiridaz have been published, whole-body PET images at multiple time points also showed that the liver began to washout significantly after 50–70 min, and the radioactive activity in the blood pool increased correspondingly [25]. The cumulative urine excretion of XTR004 and flurpiridaz was similar [25], which was 8.18%ID for XTR004 within 7.25 h (range: 1.04–23.0%ID; %CV: 180.1), and 4.83%ID for flurpiridaz over 7 h (range: 0.64–12.41%ID; %CV: 64.7).

Radiation Dosimetry

The top five organs of XTR004 after IV injection were thyroid (54.9 μSv/MBq), kidney (49.53 μSv/MBq), liver (49.23 μSv/MBq), myocardium (45.16 μSv /MBq), and bladder wall (44.59 μSv/MBq). The top organs of flurpiridaz [25] included kidney (66μSv/MBq) and myocardium (48 μSv/MBq). The whole-body effective dose of XTR004 was 0.0165 mSv/MBq as slightly lower than that of flurpiridaz (0.0189 mSv/MBq). With the actual injected dose of 270.27 MBq (7.30 mCi of injection activity), the corresponding who-body effective radiation dose was 4.474 mSv, which is close to that of flurpiridaz and other PET MPI tracers (Table 5) [25, 34].

Table 5
Radiation dose of MPI tracers injected at rest, compared to that of XTR004

Parameter	^{201}Tl [25]	^{99m}Tc-sestamibi [25]	^{99m}Tc-tetrofosmin [34]	^{82}Rb-2-Dimensional bismuth germanate [25]	^{82}Rb-3-Dimensional bismuth germanate [25]	^{13}N-ammonia [34]	^{15}O-H_2O [34]	Flurpiridaz [25]	XTR004
Rest dose (MBq)	111	370	740	1850	555	740	2220	111	270
Critical organ	Ovaries	Gallbladder	Gallbladder	Kidneys	Kidneys	Urinary bladder	Heart wall	Kidneys	Thyroid
Critical organ dose per rest study (mSv)	81	14	26.64	10.8	3.2	5.99	4.22	7.3	14.97
ED per rest study(mSv)	24	3.3	5.6	2.3	0.7	1.5	2.1	2.1	4.47
Critical organ dose per rest study (mSv/MBq)	0.7297	0.0378	0.036	0.0058	0.0058	0.0081	0.0019	0.0658	0.0554
ED per rest study(mSv/MBq)	0.2162	0.0089	0.0076	0.0012	0.0013	0.002	0.0009	0.0189	0.0165

Safety

During the entire trial, no SAE occurred was observed and no clinically significant safety issues were found. TRAE occurred in seven subjects (63.6%), all of whom had mild pain at the injection site, mainly due to the study drug containing little alcohol (10% injection volume, 0.1–0.5 mL). No measures were taken for any TRAE, and the patients were cured without treatment at the end of the study. In the Phase I clinical study of flurpiridaz, there was no occurrence of SAE, and three subjects (23% of the total) had drug-unrelated AE, which were nausea, fatigue, and needle-like contusion. All AEs were mild and did not require treatment [25]. XTR004 has a good safety profile compared to data from flurpiridaz.

Limitations Of The Study

Due to the detectable limits of the radio-HPLC instrument in this study, the proportion of prototype in urine data could not be obtained; therefore, the level of metabolites in urine was unknown. Upon the same reason, the level of metabolites in plasma after 120 minutes was also unknown. In future studies, the use of more sensitive radio-HPLC instrument should be considered to fully study metabolites in plasma and urine accordingly.

Conclusion

XTR004 having a favorable safety profile with rapid, high, and stable myocardial uptake in humans demonstrated an excellent potential for PET MPI. Further exploration of XTR004 PET MPI to detect myocardial ischemia can be warranted.

Declarations

Acknowledgement

The authors appreciate the excellent technical assistance of the staff at the Department of Nuclear Medicine, Peking Union Medical College Hospital, Chinese Academy of Medical Sciences and Peking Union Medical College, and the staff at Medical Department, Sinotau Pharmaceutical Group.

Funding

This work was sponsored in part by CAMS innovation fund for medical science (No. CIFMS-2022-I2M-JB-001, CIFMS-2021-I2M-1-02, CIFMS-2021-I2M-1-002, CIFMS-2021-I2M-1-003); National Key Research and Development Program of China (No. 2016YFC0901500); National High Level Hospital Clinical Research Funding (XH-QN-012K, 2022-PUMCH-D-001); Beijing Municipal Commission of Science and Technology (Z191100007619001).

Author Contribution

Li Huo, Bailing Hsu designed this study and organized the data collection, Qingqing Pan, Chao Fu, Peipei Wang, Zhiquan Zheng collected the data, Chao Ren, Qingqing Pan processed and analyzed the data, Chao Ren and Li Huo lead the manuscript writing, all authors reviewed and revised the manuscript.

Data Availability

Datasets generated during and/or analyzed during the current study are available from the corresponding author upon reasonable request.

Conflict of Interest

Chao Ren Qingqing Pan Chao Fu Peipei Wang Li Huo have received consulting fees or honoraria; Zhiquan Zheng is currently an employee of Sinotau Pharmaceutical Group; Bailing Hsu received royalty from Sinotau Pharmaceutical Group.

Ethical Approval

All procedures performed in studies involving human participants were in accordance with the ethical standards of the institutional and/or national research committee and with the 1964 Helsinki declaration and its later amendments or comparable ethical standards.

References

1. Roth GA, Mensah GA, Johnson CO, et al. Global Burden of Cardiovascular Diseases and Risk Factors, 1990–2019: Update From the GBD 2019 Study. J Am Coll Cardiol. 2020 Dec;22(25):2982–3021. 76(.
2. Tsao CW, Aday AW, Almarzooq ZI, et al. Heart Disease and Stroke Statistics-2022 Update: A Report From the American Heart Association. Circulation. 2022 Feb;22(8):e153–639. 145(.
3. The Writing Committee of the Report on Cardiovascular Health. and Diseases in China. Report on Cardiovascular Health and Diseases in China 2021: an Updated Summary. Chin Circulation J. 2022;36:553–78.
4. Zhou M, Wang H, Zeng X, et al. Mortality, morbidity, and risk factors in China and its provinces, 1990–2017: a systematic analysis for the Global Burden of Disease Study 2017. Lancet. 2019 Sep;28(10204):1145–58. 394(.
5. Fihn SD, Gardin JM, Abrams J, et al. American College of Cardiology Foundation. 2012 ACCF/AHA/ACP /AATS/PCNA/SCAI/STS guideline for the diagnosis and management of patients with stable ischemic heart disease: executive summary: a report of the American College of Cardiology Foundation/American Heart Association task force on practice guidelines, and the American College of Physicians, American Association for Thoracic Surgery, Preventive Cardiovascular Nurses Association, Society for Cardiovascular Angiography and Interventions, and Society of Thoracic Surgeons. Circulation. 2012 Dec 18;126(25):3097 – 137.
6. Members TF, Montalescot G, Sechtem U, et al. 2013 ESC guidelines on the management of stable coronary artery disease: the Task Force on the management of stable coronary artery disease of the European Society of Cardiology. Eur Heart J. 2013 Oct;34(38):2949–3003.
7. Knuuti J, Wijns W, Saraste A, et al. ESC Scientific Document Group. 2019 ESC Guidelines for the diagnosis and management of chronic coronary syndromes. Eur Heart J. 2020 Jan 14;41(3):407–477.
8. Kunadian V, Chieffo A, Camici PG, et al. An EAPCI Expert Consensus Document on Ischaemia with Non-Obstructive Coronary Arteries in Collaboration with European Society of Cardiology Working Group on Coronary Pathophysiology & Microcirculation Endorsed by Coronary Vasomotor Disorders International Study Group. Eur Heart J. 2020 Oct 1;41(37):3504–3520.
9. Henzlova MJ, Duvall WL, Einstein AJ, et al. ASNC imaging guidelines for SPECT nuclear cardiology procedures: Stress, protocols, and tracers. J Nucl Cardiol. 2016 Jun;23(3):606–39.
10. Danad I, Raijmakers PG, Driessen RS, et al. Comparison of Coronary CT Angiography, SPECT, PET, and Hybrid Imaging for Diagnosis of Ischemic Heart Disease Determined by Fractional Flow Reserve. JAMA Cardiol. 2017 Oct 1;2(10):1100–1107.

11. Jaarsma C, Leiner T, Bekkers SC, et al. Diagnostic performance of noninvasive myocardial perfusion imaging using single-photon emission computed tomography, cardiac magnetic resonance, and positron emission tomography imaging for the detection of obstructive coronary artery disease: a meta-analysis. J Am Coll Cardiol. 2012 May 8;59(19):1719-28.
12. Murthy VL, Bateman TM, Beanlands RS, et al. Clinical Quantification of Myocardial Blood Flow Using PET: Joint Position Paper of the SNMMI Cardiovascular Council and the ASNC. J Nucl Med. 2018 Feb;59(2):273–93.
13. Di Carli MF. Why Will PET Be the Future of Nuclear Cardiology? J Nucl Med. 2021 Sep;1(9):1189–91. 62(.
14. Le Guludec D, Lautamäki R, Knuuti J, et al. European Council of Nuclear Cardiology. Present and future of clinical cardiovascular PET imaging in Europe–a position statement by the European Council of Nuclear Cardiology (ECNC). Eur J Nucl Med Mol Imaging. 2008 Sep;35(9):1709–24.
15. Brunken RC. Promising New 18F-Labeled Tracers for PET Myocardial Perfusion Imaging. J Nucl Med. 2015 Oct;56(10):1478–9.
16. Beller GA, Watson DD. A welcomed new myocardial perfusion imaging agent for positron emission tomography. Circulation. 2009 May 5;119(17):2299–301.
17. Liga R, Neglia D. Emerging. F-18-Labelled PET Myocardial Perfusion Tracers. Curr Cardiol Rep. 2020 Aug 9;22(10):116.
18. Yalamanchili P, Wexler E, Hayes M, et al. Mechanism of uptake and retention of F-18 BMS-747158-02 in cardiomyocytes: a novel PET myocardial imaging agent. J Nucl Cardiol. 2007 Nov-Dec;14(6):782–8.
19. Maddahi J, Packard RR. Cardiac PET perfusion tracers: current status and future directions. Semin Nucl Med. 2014 Sep;44(5):333–43.
20. Berman DS, Maddahi J, Tamarappoo BK, et al. Phase II safety and clinical comparison with single-photon emission computed tomography myocardial perfusion imaging for detection of coronary artery disease: flurpiridaz F 18 positron emission tomography. J Am Coll Cardiol. 2013 Jan;29(4):469–77. 61(.
21. Maddahi J, Lazewatsky J, Udelson JE, et al. Phase-III Clinical Trial of Fluorine-18 Flurpiridaz Positron Emission Tomography for Evaluation of Coronary Artery Disease. J Am Coll Cardiol. 2020 Jul;28(4):391–401. 76).
22. Mou T, Zhao Z, You L, et al. Synthesis and Evaluation of (18)F-labeled Pyridaben Analogues for Myocardial Perfusion Imaging in Mice, Rats and Chinese mini-swine. Sci Rep. 2016 Sep;20:6:33450.
23. Mou T, Zhang X. Research Progress on 18F-Labeled Agents for Imaging of Myocardial Perfusion with Positron Emission Tomography. Molecules. 2017 Mar;30(4):562. 22(.
24. Loening AM, Gambhir SS. AMIDE: a free software tool for multimodality medical image analysis. Mol Imaging. 2003 Jul;2(3):131–7.
25. Maddahi J, Czernin J, Lazewatsky J, et al. Phase I, first-in-human study of BMS747158, a novel 18F-labeled tracer for myocardial perfusion PET: dosimetry, biodistribution, safety, and imaging characteristics after a single injection at rest. J Nucl Med. 2011 Sep;52(9):1490–8.
26. Ballabh P, Braun A, Nedergaard M. The blood-brain barrier: an overview: structure, regulation, and clinical implications. Neurobiol Dis. 2004 Jun;16(1):1–13.
27. Savi A, Gerundini P, Zoli P, et al. Biodistribution of Tc-99m methoxy-isobutyl-isonitrile (MIBI) in humans. Eur J Nucl Med. 1989;15(9):597–600.
28. Yi C, Yu D, Shi X, et al. Biodistribution and estimation of radiation-absorbed doses in humans for 13N-ammonia PET. Ann Nucl Med. 2015 Nov;29(9):810–5.
29. Hunter CRRN, Hill J, Ziadi MC, et al. Biodistribution and radiation dosimetry of 82 Rb at rest and during peak pharmacological stress in patients referred for myocardial perfusion imaging. Eur J Nuclear Medicine&Molecular Imaging. 2015;42:1032–42.
30. Smith T, Tong C, Lammertsma AA, et al. Dosimetry of intravenously administered oxygen-15 labelled water in man: a model based on experimental human data from 21 subjects. Eur J Nuclear Medicine&Molecular Imaging. 1994;21:1126–34.
31. Otaki Y, Van Kriekinge SD, Wei CC, et al. Improved myocardial blood flow estimation with residual activity correction and motion correction in 18F-flurpiridaz PET myocardial perfusion imaging. Eur J Nucl Med Mol Imaging. 2022 May;49(6):1881–93.
32. Moody JB, Poitrasson-Rivière A, Hagio T, et al. Added value of myocardial blood flow using 18F-flurpiridaz PET to diagnose coronary artery disease: The flurpiridaz 301 trial. J Nucl Cardiol. 2021 Oct;28(5):2313–29.
33. Dilsizian V. Transition from SPECT to PET myocardial perfusion imaging: A desirable change in nuclear cardiology to approach perfection. J Nucl Cardiol. 2016 Jun;23(3):337–8.
34. Stabin MG. Radiopharmaceuticals for nuclear cardiology: radiation dosimetry, uncertainties, and risk. J Nucl Med. 2008 Sep;49(9):1555–63.

Figures

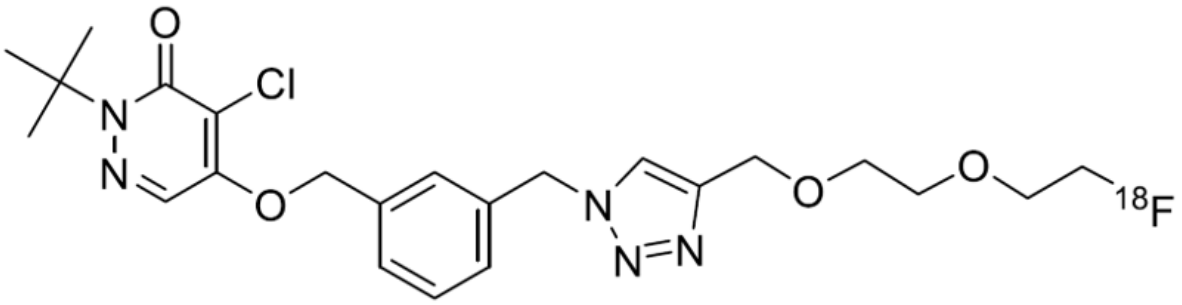

Figure 1

Chemical structure of XTR004.

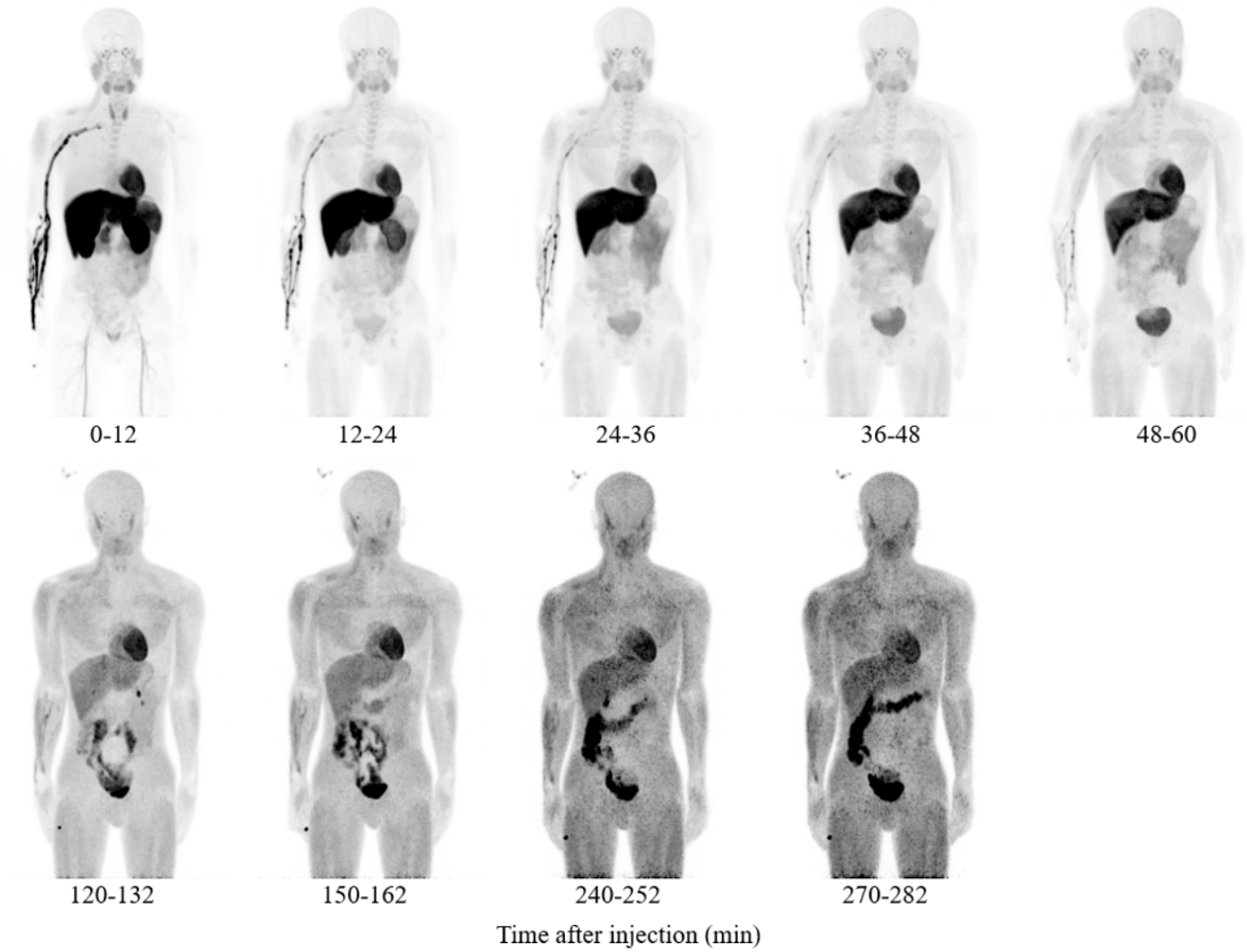

Figure 2

Max intensity projection of whole-body PET images in the coronal view at different time points after administration of XTR004 from a representative subject. PET images have been corrected for ^{18}F decay.

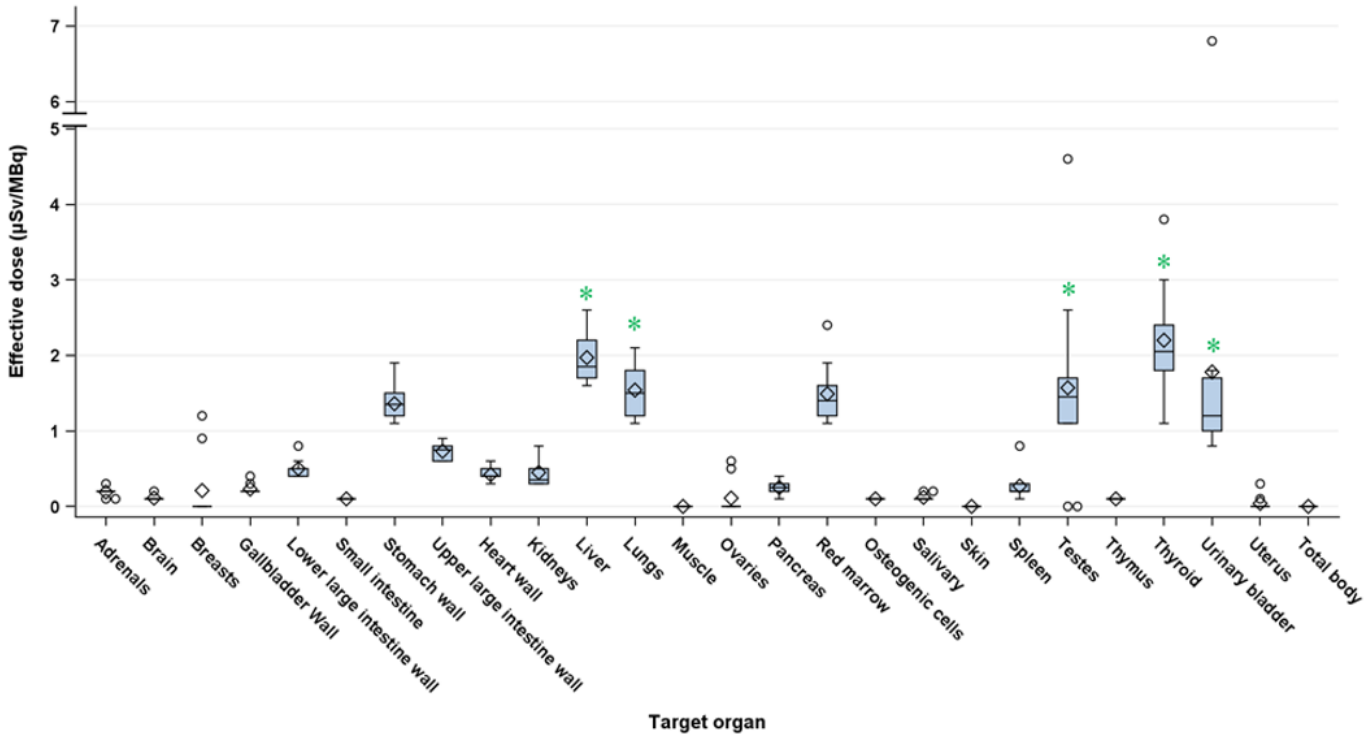

Figure 3

Boxplots of effective radiation doses of organs and whole-body after IV injection of XTR004. Top five organs are: thyroid (2.20 µSv/MBq), liver (1.97 µSv/MBq), bladder wall (1.78 µSv/MBq), testes (1.57 µSv/MBq), and lungs (1.54 µSv/MBq).

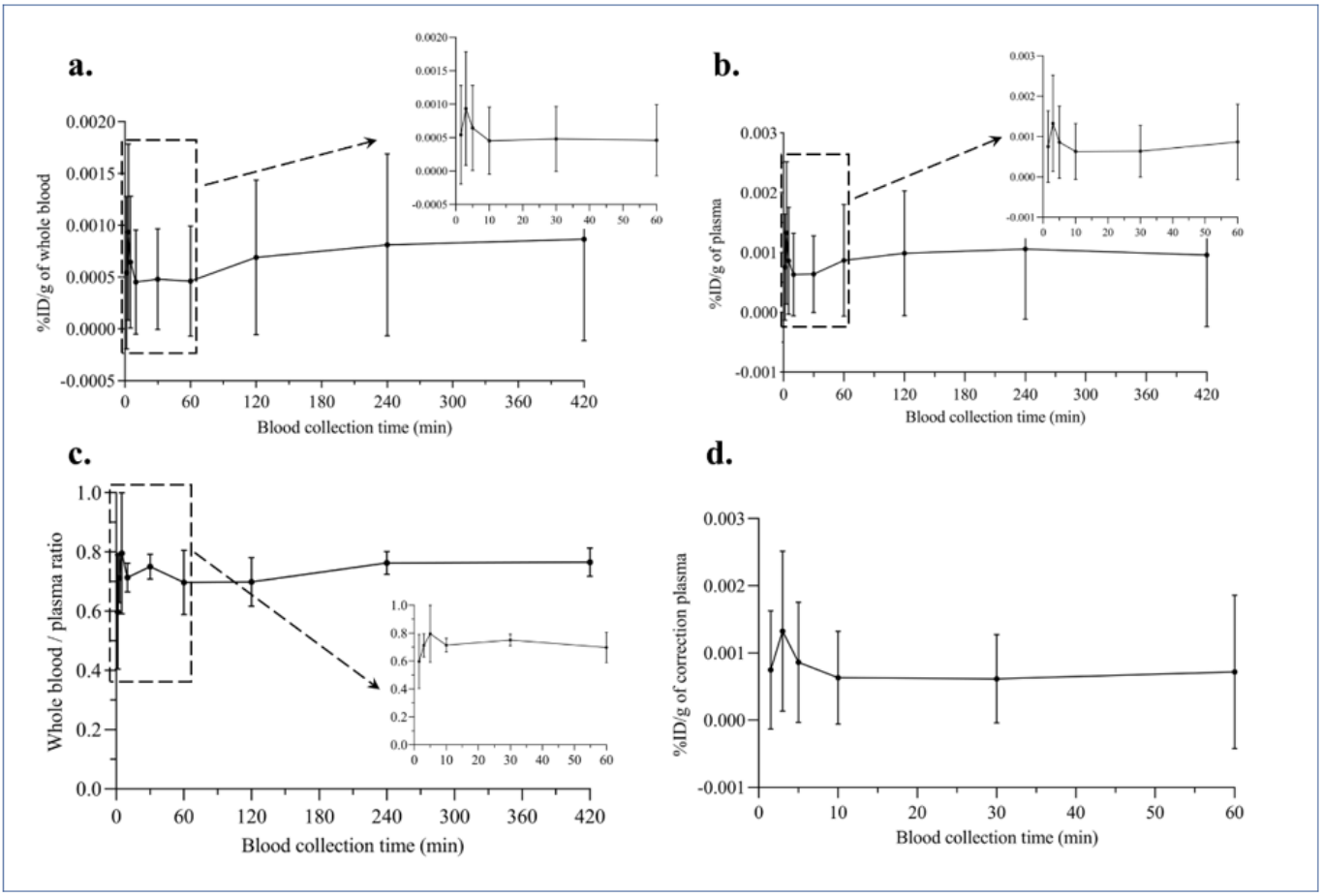

Figure 4

Time activity curves (TAC) of radioactive concentrations in whole-blood, plasma and metabolism-corrected plasma. a) TAC of whole-blood, b) TAC of plasma, c) the radioactivity concentration ratio of whole blood and plasma and d) TAC of the metabolite-corrected plasma.

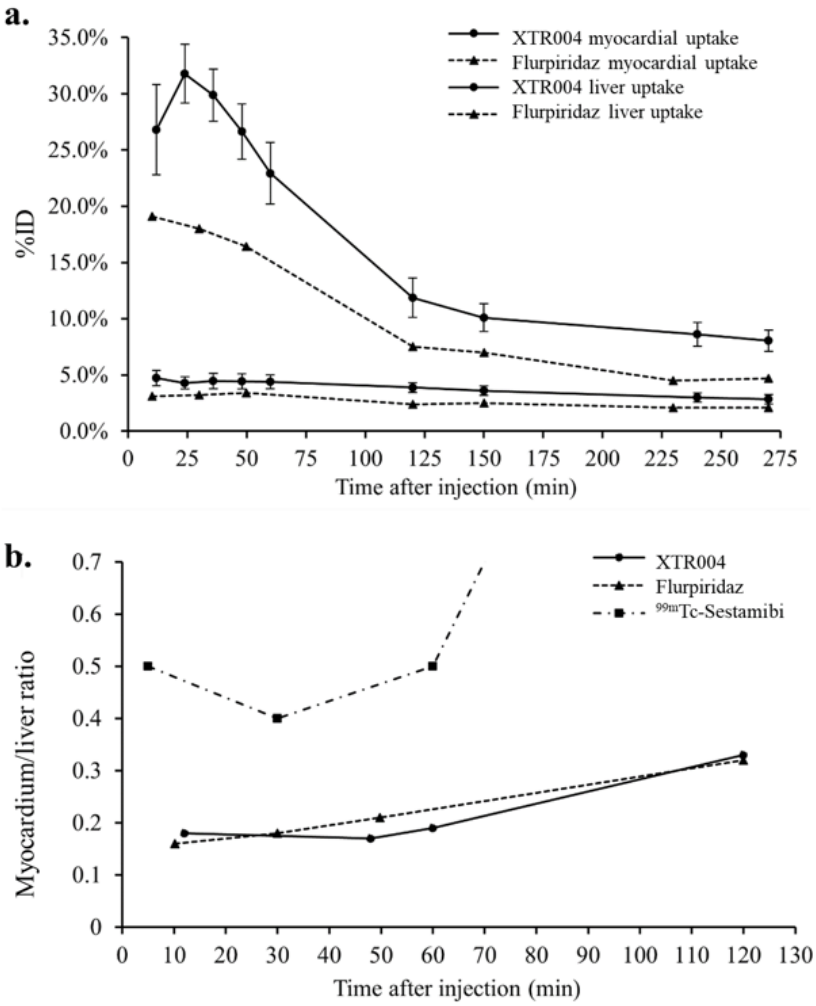

Figure 5

Myocardial and liver uptake of XTR004 and flurpiridaz over time after IV injection. a.) myocardial and liver uptake, b) myocardium/liver ratio of XTR004, flurpiridaz and ^{99m}Tc-Sestamibi.